5

Particle Size Distribution and Zeta Potential Based on Dynamic Light Scattering: Techniques to Characterize Stability and Surface Charge Distribution of Charged Colloids

SANAT KARMAKAR

ABSTRACT

Size distribution and zeta potential based on dynamic light scattering (DLS) are the essential characterizations prior to any applications of some charged colloids. Nowadays, these are the routine methods used in a wide variety of research areas, such as, stability of nanoparticles, colloids, bio-colloids and polymer science etc. In this chapter, the basic techniques, principles and data analysis will be discussed in details. First, theory, experiment, data analysis and inference from DLS techniques will be discussed. Next, we shall discuss zeta potential as a tool to characterize the stability and surface charge distributions of charged colloids. Some examples of usages of these techniques in material science will also be discussed.

Key words: Dynamic light scattering, Zeta potential, Colloids, Surface charge, Electrophoresis, Debye length

Light scattering from a matter is widely used non-invasive technique with applications in numerous scientific disciplines[1]. The specific

Soft matter and Biophysics Laboratory, Department of Physics, Jadavpur University, Kolkata – 700032, India

* *Corresponding author*: E-mail: sanatkarmakar@gmail.com

properties of the molecules can be studied depending on the light source and the detector used. In 1859, the scattering of light, observed by John Tyndall in colloids, is one of the earliest light scattering experiments[2]. Later in 1904, the Lord Rayleigh explained the blue colour of the sky, which is caused by the light scattering from smaller atmospheric particles with respect wavelengths of light. This result established the fact that the refractive index of the medium plays a vital role in light scattering phenomenon. In the early twentieth century, Gustav Mie (1908) established the theory to investigate the light scattering from absorbing and non-absorbing media containing particles that are larger compared to the wavelength of light[3]. The Mie theory also takes into account particle shape and the contrast in refractive index between particles and the medium in which particles are suspended. However, Peter Debye suggested that the scattering of particles can be studied independently of assumptions on mass, size, or shape as a function of angle, which is often referred to as Rayleigh–Debye scattering[4]. Detection and analysis of absolute mean intensity as a function of scattering angle is known as static light scattering (SLS). On the other hand, intensity fluctuations of scattered light provide information on the dynamics of the systems. The measurement and analysis of such intensity fluctuations to obtain the material properties is termed as dynamic light scattering (DLS). In the present chapter we shall discuss only the various aspects of DLS.

The DLS technique provides us the information about the material properties at "long wavelength" limited by the wavelength of light. This technique is a consequence of the interaction of light with particles and often known as photon correlation spectroscopy (PCS) and quasi–elastic light scattering[5]. DLS mostly uses the Mie theory of scattering to estimate the particle size[3]. Information, such as, size of the particles, molecular weight, diffusion constant, interaction length, second virial coefficient etc are obtained. This technique is also used to obtain the electrostatics and the dynamic behaviour of charged particles in a solution. Zeta potential is one such property of charged colloids which can be measured from a technique known as laser Doppler velocimetry along with phase analysis light scattering based on DLS[6]. In contrast to DLS, other scattering techniques, such as x-ray or neutron provide us information at much shorter length scale typically of inter-atomic distances (Table 1)[7]. Scattering of light can occur whenever there are variations of refractive index within the materials, whereas, x-ray (much shorter wavelength compared to visible light) scattering depends on contrast in the electron density of the materials. Spatial variation of refractive index of the materials leads to static scattering where one

measures the intensity as a function of scattering angle. The intensity fluctuations of scattered light with time give us information on the dynamics of the particles in solution. In dynamic light scattering (DLS), the intensity fluctuations with time are measured to obtain the size information.

DLS is widely used to analyze size distributions of nano-particles, proteins, latex and colloids[8]. DLS provides us with an understanding of stability as well as the dynamics of nano and micron-sized particles. Nowadays, this technique has drawn a significant attention for biomedical applications[9]. The dynamic light-scattering technique has a number of advantages over other experimental methods. For instance, it is possible to perform experiments with a wide range of sample buffer and wide range of temperature as well as concentrations. DLS is also a non-invasive technique that requires comparatively low amounts of sample and provides reliable estimates of the quality of preparation rapidly.

Table 1: Different scattering techniques for the determination of the structure of the materials at various length scale.

Techniques	Wavelength	Energy	Information
X-rays (Synchrotron)	~1-10A	~KeV	Atomic structure and also Large scale (~10-100A) structure (SAXS)
Neutron (Reactor)	~1-20A	~MeV	Structure and internal dynamics
Light (Laser)			Structure (SLS) Dynamic (DLS) ⇓ Photon correlation spectroscopy

In this chapter, we will discuss the basic principle of dynamic light scattering and its uses to characterize micron or even nano-sized particles. First, we discuss the detailed experimental technique to determine the size distributions of particles and then we discuss the measurement of electrophoretic mobility for charged colloids. Electrophoretic mobility provides information about the zeta potential which is a good approximation of surface potential of the charged particles in solution. The knowledge of zeta potential also provides us the electrostatic interactions and stability of the particles in a solution.

1. DYNAMIC LIGHT SCATTERING TO CHARACTERIZE THE DIFFUSION OF PARTICLES IN SOLUTION

The relation between the diffusion behavior of particles in solution and dynamic light scattering was established by a series of seminal discoveries. The theory of Brownian motion was explained by Smoluchowski assuming the kinetic model of colliding spheres[10]. This theory results how fluctuations give rise to an appreciable effect when the effect of an individual collision is negligible. On the other hand, a similar result was obtained by Einstein assuming the probabilistic aspect instead of kinetic consideration. The mean square displacement of the particles estimated from Brownian motion is directly proportional to time. Further, Langevin theory and more generalized theory given by Fokker and Planck establish the diffusion equation from Brownian motion. Later, Einstein also established that Brownian motion can be mapped into the diffusion problem. The relationship between the diffusion coefficients of particles to their translational friction along with the discovery from Sir George Stokes (1845) suggested that the friction exerted by a moving particle is proportional to its radius and to the viscosity of the solvent surrounding particles[11]. The density and the concentration fluctuations of the particles in a solution due to Brownian motion lead to intensity fluctuations in the scattered light when a monochromatic light beam encounters the system.

Dynamic light scattering (DLS) measures the particle size in sub-micron regime from the intensity fluctuations of the scattered lights. Translational diffusion is strongly dependent on the temperature and viscosity of the medium in which particles are dispersed. The root mean square displacement of the particle relates the diffusion constant which in turn allows us to estimate the particle size *via* Einstein stokes relation[12]. The intensity fluctuations of scattered light determine the intensity-intensity correlation function which can be used to obtain the diffusion coefficient and hence the particle size in the system. Over the years, there have been a number of experimental and theoretical approaches to determine the diffusion coefficient of particles in a solution which eventually lead to the development of modern DLS instruments[13-17]. Let us discuss the theory of DLS, which will tell us how the measured intensity autocorrelation is related to diffusion constant as well as particle size distributions.

1.1 Theory of Dynamic Light Scattering

When a monochromatic light typically laser beam is incident on a sample, scattering of light occurs due to local fluctuations of refractive

index of the medium. Usually the refractive index of the particles is different from the solvent. Light is primarily scattered by particles suspended in a solution executing Brownian motion. Intensity fluctuations of scattered light are measured and analyzed to obtain diffusion constant and hence the hydrodynamic radius of the particle. The movement of particles in a solution depends on their size, temperature, and solvent viscosity[18]. It has been well established that for a fixed temperature and solvent viscosity, the larger particles diffuse slowly compared to smaller particles. As the intensity fluctuations of the scattered light occur as a result of local particle density fluctuations due to Brownian motion, the intensity fluctuation also appears to be very rapid for smaller particles relative to larger particles as described in Fig. 1. The continuous Brownian fluctuation of the molecules causes frequency shift of the monochromatic incident light and the amount of shift depends on the size of particles. This phenomenon is known as Doppler broadening. The spread of frequencies, $\Delta\omega$, is dependent on the diffusion coefficient D as $\Delta\omega = Dq^2$, where q is the scattering vector.

In a typical scattering experiment, intensity fluctuations, measured at two different times t and $t + \tau$, look like a statistical noise. However, If τ is much smaller than the characteristic time of fluctuation, these intensities measured in the time interval τ are correlated. Therefore, we define intensity auto correlation function as

$$\langle I(t_0)\, I(t_0+\tau)\rangle = \lim_{T\to\infty} \frac{1}{T} \int_{t_0}^{T} I(t) I(t+\tau) dt = G(\tau) \qquad (1)$$

Since t_0 is Wthe initial or starting time and can be taken as t_0=0. Average of intensity – intensity data was taken over the duration of the experiments. In DLS, the amplitude fluctuations of the electric field can be described in term of normalized correlation function.

$$g_1(q,t) = \frac{\langle E_{Sc}(q,t\ )\, E_{SC}(q,t+\tau)\rangle}{< |E_{Sc}(q,t)|^2 >} \qquad (2)$$

where $\langle E_S(q,t\ )\rangle$ is the scattering amplitude.

Now, consider light is incident on a system of N particles. Now the electric field of the incident light can be represented as $E_{inc} = A\, e^{-i\, k_{in}.r_j}$. The electric field of the scattered light from the j^{th} particle at position r_j(t) is given by $E_S(t) = B_j e^{-i\,(k_{in}-k_s).r_j(t)} = B_j e^{-i\,q.r_j(t)}$, where q is the

scattering vector of magnitude $\frac{4\,\pi\ \sin\theta}{\lambda}$. For system of N particles we can obtain the scattering amplitude as

$$E_{Sc}(t) = \sum_{j=1}^{N} B_j\ e^{-i\ q.r_j(t)} \tag{3}$$

Normalized field autocorrelation function

$$g_1(\tau) = \frac{\langle \sum_{j=1}^{N} B_j\ e^{-i\ q.r_j(t)} \sum_{k=1}^{N} B_k\ e^{-i\ q.r_k(t+\tau)} \rangle}{\langle |\sum_{j=1}^{N} B_j\ e^{-i\ q.r_j(t)}|^2 \rangle} \tag{4}$$

$$g_1(\tau) = \langle e^{-i\ q.\Delta r\ (\tau)} \rangle = F(q,\tau) \tag{5}$$

The particle distribution function can be defined as
$f(r,\tau) = \langle \delta(\ r - \{r_j(\tau) - \ r_j(0)\} \rangle$

Now the scattering amplitude is the Fourier transform of $f(r,\tau)$. Therefore, the intensity autocorrelation function is the Fourier transformation of the power spectrum, and therefore the DLS measurements can be equally well performed in the spectral domain[19].

$$F(q,\tau) = \int_0^{\infty} e^{-iq.r}\ f(r,\tau) d^3r \tag{6}$$

According to the theory of Brownian motion, $f(r,\tau)$ satisfies the diffusion equation.

$$\frac{\partial f(r,\tau)}{\partial \tau} = D\nabla^2 f(r,\tau) \tag{7}$$

where, D is the diffusion constant. By Fourier transforming the equation 7 equation we get

$$\frac{\partial F(q,\tau)}{\partial \tau} = D\mathrm{q}^2 F(q,\tau) \tag{7a}$$

Solution of the equation 7a gives

$$F(q,\tau) = \ e^{-Dq^2\tau} \tag{8}$$

Therefore, $g_1(\tau) = e^{-Dq^2\tau}$. The electric field correlation, $g_1(\tau)$ decays exponentially and is dependent on a decay constant, $\Gamma = Dq^2$, for

monodisperse particles undergoing a Brownian motion. G(τ) is related to $g_1(\tau)$ *via* the Siegert relation based on an approximation that the photodetector detects only the scattered light and that the photon counting is a random Gaussian process. Therefore, the intensity-intensity autocorrelation function can be written as

$$G(\tau) = A + \beta|g_1(\tau)|^2 = A + \beta e^{-2Dq^2\tau} \quad (9)$$

where β is the coherence factor that depends on detector area, optical alignment, and the scattering properties of macromolecules. A is the baseline and can be normalized to a value 1. It is important to mention here that, for a polydisperse sample, $g_1(\tau)$ cannot be represented as a single exponential decay rate Γ, but can be expressed as the intensity weighted average of distribution of decay rate $G(\Gamma)$. In this case, $g_1(\tau) = \int_0^\infty G(\Gamma)e^{-\Gamma\tau}\, d\Gamma$. The equation (9) is used to fit the measured intensity autocorrelation function to obtain the diffusion constant D. The size of the particles in terms of hydrodynamic radius (R_h) has been estimated using the Einstein - Stoke relation.

$$R_h = \frac{kT}{6\,\pi\eta D} \quad (10)$$

Where kT being the thermal energy (k: Boltzmann constant, T: temperature in ºK) and be the coefficient of viscosity of the medium (k = 1.38 × 10^{-23} Joule/Kelvin). Hydrodynamic radius refers to the radius of the sphere that diffuses with the same velocity as that of the particle. Now the frictional coefficient C can be expressed as = $\frac{kT}{D}$. The frictional coefficient can also be written using equation (10) as

$$C = 6\pi\eta R_h \quad (11)$$

Theory of DLS assumes only spherical particles. Therefore, deviation from spherical shape can be envisaged from measured frictional coefficient (equation (11)) when compared with the frictional coefficient of unsolvated volume of the particle (actual radius sphere).

1.2 Experiment

In a typical DLS experiment, laser light is used to illuminate the sample cuvette. Red He-Ne or semiconductor laser of wavelength 630 nm and power of 2–4 mW is used. The sample must be filtered to eliminate the

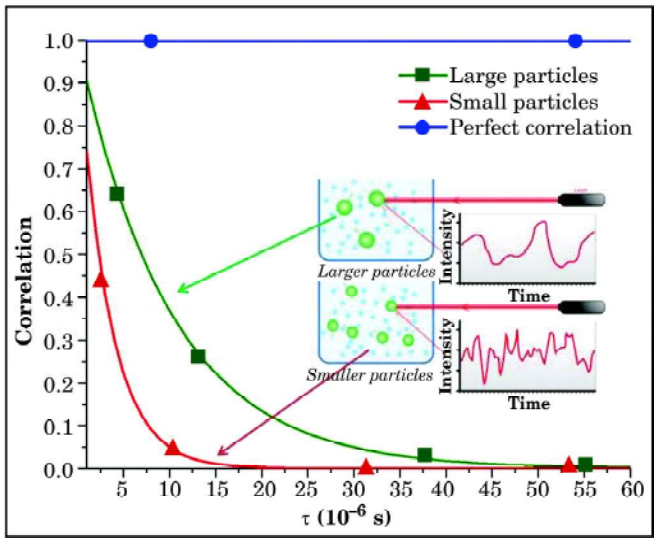

Fig. 1: Schematic representation of the relation between particle size and intensity fluctuations and hence the correlation function.

unwanted larger particles. In the dilute limit most of the laser beam passes through the sample and some are scattered by the particles. The scattered light is then detected by either the photo detector or avalanche photo diode. If the concentration of the particle is very large, then too much scattered light will be detected. In this situation, an attenuator is placed before the sample (as shown in Fig. 2) to reduce the incident laser intensity to a desired intensity. In a DLS experiment, scattered intensities are measured at a fixed scattering angle, typically at 90° or 173° (*i.e.*, back scattered light). It is important to mention that the rotational diffusion of molecules will affect the observed autocorrelation function. The effect of rotational diffusion on the observed autocorrelation function can be ignored when scattered light is detected at 173° (*i.e.*, the back scattered light) compared to the detection at 90°. Therefore, by detecting the back scattered light only the translational diffusion D can be obtained. Detection of back scattered light also allows minimizing multiple scattering by the sample and hence it is possible to use high concentration sample for DLS measurement. Further, scattering from unwanted large dust particles present in the solution is mostly in the forward direction compared to the smaller particles which scatter almost equally in all directions. Modern light scattering instruments, such as zetasizer nano ZS (Malvern Instrument, UK) have provision for detection of scattered light at 90° as well as 173°.

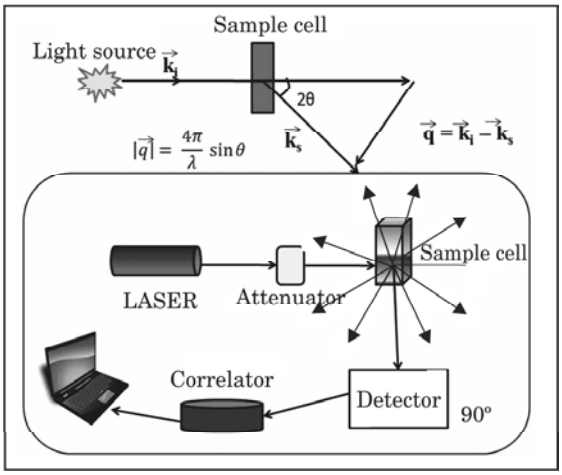

Fig. 2: Schematic representation of scattering geometry and experimental setup for dynamic light scattering experiment. Here $\vec{k_i}$ and $\vec{k_s}$ are the incident and scattered wave vectors and q is the resultant scattering vector whose magnitude is given in the figure.

The scattered signals from the detector are then fed to the digital correlator. The rate of intensity fluctuations is monitored by the correlator which compares the scattered intensity at successive time intervals. Correlator is connected to a computer which provides the correlation curve G (τ) *vs.* τ. Sample properties, such as dispersant viscosity and refractive index are required to calculate the size distribution. For better DLS result, the sample should be transparent to light. However, for efficient scattering, it is essential to have sufficient contrast in the refractive indices between the particle and the dispersant. The concentration of the sample depends on the particle size and refractive index of the dispersant. Therefore, the choice of concentration of the sample is important in order to obtain efficient scattering from particles. Excessive diluted particle dispersion will give us a poor signal to noise ratio. However, the lower limit of concentration depends on the laser power, detector sensitivity and optical configuration of the instrument. Concentrated particle dispersion should also be avoided in order to restrict multiple scattering. High concentration of sample will hinder free diffusion of the particles due to interparticle interaction, leading to restricted Brownian motion. Therefore, in order to determine the optimum desired concentration, one would like to perform a series of size measurement as a function of concentration. The experiments should be performed over a certain range of the concentration for which average distributions of particle size do not alter significantly.

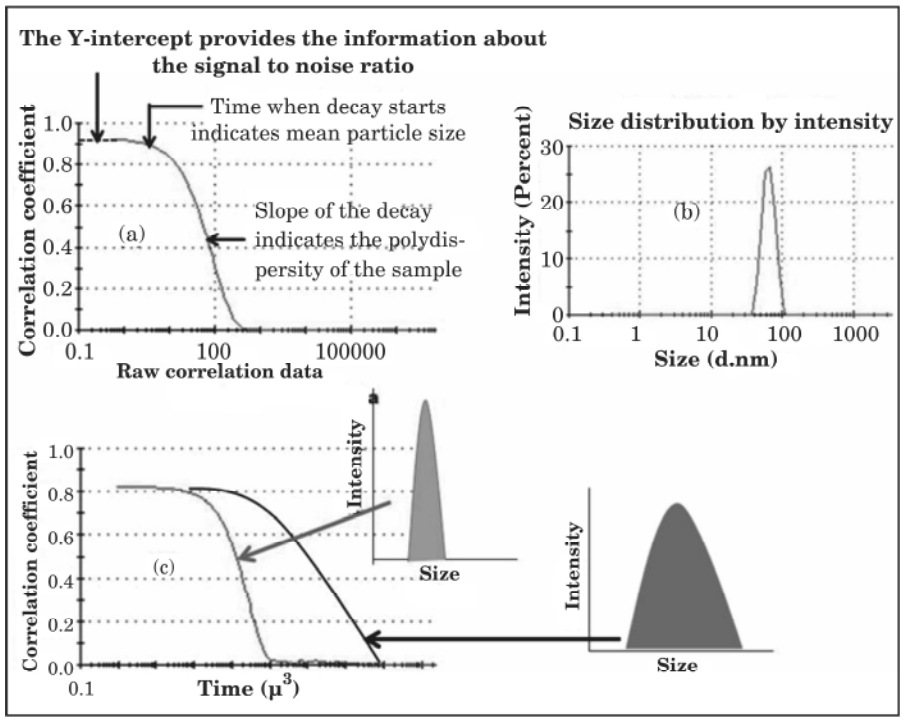

Figs. 3: Interpretation of the correlation curve obtained from intensity fluctuations is illustrated in Figs. a-b shows the typical size distribution obtained from cumulant analysis of the correlation data. The analysis essentially provides the mean size and polydispersity index. Time, when decay of the correlation function starts indicates the mean size of the particle. Therefore, decay starts at larger time for larger particles than smaller particles. Fig. c corresponds to much larger particles compared to (a). However, the rate of decay, *i.e.*, the slope or gradient of decay determines the polydispersity of the size distribution. Larger the slop greater the polydispersity of the sample, as reflected in the width of the size distribution depicted in (c). The width of the size distribution is a measure of polydispersity and quantitative measure of polydispersity is discussed section 1.3. The value of Y- intercept is normalized to one for ideal signal.

1.3 Interpretation of Data

The correlation function (equation 9) contains all information regarding the diffusion of particles in a solution. In order to obtain reliable information on diffusion coefficient, two approaches are widely used to fit the correlation function – monomodal distribution and nonmonomodal distribution methods. For a distribution with mono-disperse particles, the correlation curve appears smooth and single exponent decay function. However, for polydisperse sample or sample with different particle sizes, the correlation curve is a sum of many experimental

decays. For instance, we obtain two decay constant, corresponding to two different diffusion constants for bimodal distributions. The measured intensity auto correlation function is fitted to equation (9) to obtain the translational diffusion constant (D).

The cumulant analysis method provides mean values of the diffusion coefficient. This method was widely popular due to its ease and reliability[20], and was accepted by the International Standards Organization (ISO) in 1996 and again in 2008 (ISO, 2008).

In DLS, average size (z average) and polydispersity index (PDI) are calculated from the cumulant analysis of intensity autocorrelation functions. PDI measures the extent of polydispersity of the sample which can be envisaged from the width of the size distribution. Now, equation (9) yields

$$G(\tau) = A\left(1 + Be^{-2Dq^2\tau}\right) = A(1 + Be^{-2\Gamma\tau}) \tag{12}$$

Where, $\Gamma = Dq^2$. To account for the polydispersity or the peak broadening, we can expand the argument of the exponential part as

$$G(\tau) = A(1 + Be^{(-2\Gamma\tau + \mu\tau^2)}) \tag{13}$$

The intensity autocorrelation function is then fitted to a linearized expression obtained from equation 13.

$$y(\tau) = \frac{1}{2}\ln\{G(\tau) - A\} = \frac{1}{2}lnAB - \Gamma\tau + \frac{\mu}{2}\tau^2 = a_0 - a_1\tau + a_2\tau^2 \tag{14}$$

Here a_1 measures the intensity weighted average of mean size (Z_D) and a_2 measures the variance of the distribution and hence polydispersity *via* the relation $PDI = \frac{2a_2}{{a_1}^2}$, If we assume a single size population of a Gaussian distribution, the PDI can be directly written in term of standard deviation of the Gaussian distribution $PDI = \frac{\sigma^2}{{Z_D}^2}$.

Typical size distributions obtained from the DLS are shown in Fig. 3b. For analysis the viscosity and the refractive index of the dispersant must be known with a great accuracy. Broader the distribution, more the polydispersity of the sample. The width of the size distribution, estimated from the rate of decay is a measure of polydispersity. Unlike the cumulant analysis, non-monomodal methods are more suitable for polydisperse systems and do not assume a certain type of distribution of

diffusion properties. There are several methods developed for broad monomodal or multimodal distributions of data. The nonnegative least squares (NNLS) method[21] and constrained regularization method for inverting data (CONTIN)[22] are two most popular data analysis methods.

In the analysis of correlation statistics of time series data, the plot of autocorrelation function is often referred to as correlogram. Let us discuss the qualitative information obtained from the correlogram (Fig. 3). The smaller particle correlation curve decays at very short time scale compared to the larger particles (Figs. 3a-c). However, the slope of the decay curve depends on the polydispersity of the particle (Fig. 3c). If the particles are highly monodisperse, the decay is very fast, *i.e.*, the correlation curve becomes very stiff. Therefore, the rate of decay, *i.e.*, the slope of the correlation curve provides the information about the polydispersity of the sample. The quality of data is usually determined from the signal to noise ratio. The intercept on the Y-axis in the correlogram gives information about the signal to noise ratio. For an ideal signal, the Y-intercept is normalized to a value one (Fig. 3a). Therefore, any value of Y-intercept greater than 0.9 is the best data and below 0.6 refers to a bad quality data. The photon count rate of the detector is often useful to monitor the stability as well as the quality of data. Usually attenuator is adjusted to optimize the count rate for good quality data. The Mie theory can be used to calculate the volume distribution and number distribution of the particle. Assumptions that one makes here are all particles are spherical in shape, homogeneous and equivalent density. This data are often useful when we need to compare the relative population or the amount of materials in separate peaks.

For unstable particle dispersion, the random Brownian motion will be disturbed due to sedimentation of the particles. As DLS measures the random movement of Brownian particles, it is not applicable to the non-random movement leading to sedimentation of particles. Therefore, upper size limit is strongly depends on the onset of sedimentation and number fluctuations of particles. However, DLS measurement is still applicable, if the rate of diffusion is must faster than the rate of sedimentation. A clear evidence of aggregates or sedimentation is seen in the tail of the correlogram (Fig. 4). An increase in correlation or the rapid fluctuations at high delay time, as seen in Fig. 4 is an indication of sedimentation or aggregation of particles. It is important to mention that if we observe a gradual decrease in the stable count rate over multiple measurement of the same sample , this indicates the loss of particles due to sedimentation. Such a sample may not be suitable for DLS measurement.

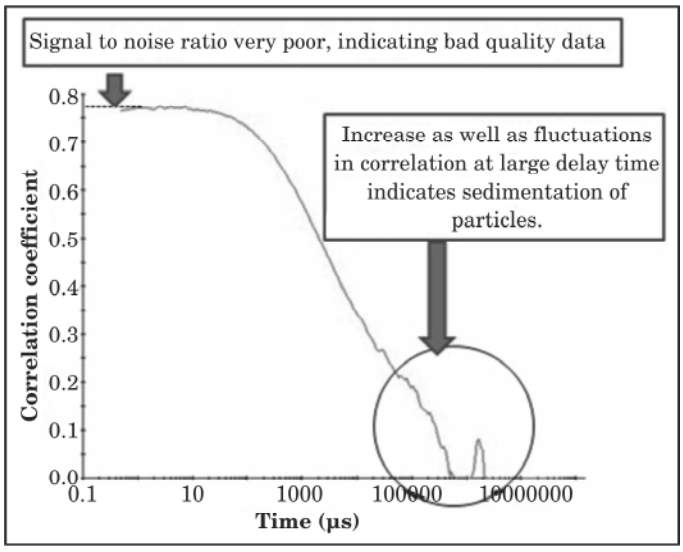

Fig. 4: Multimodal distribution of particles. The sample is too polydisperse and the clear signature of aggregation of particles is seen from the tail of the correlogram, marked by a circle. Base line (Y- intercept) in the correlogram is below 0.8, indicating poor signal to noise ratio. It is important to mention that the large fluctuations of number of particles in the measurement volume can cause elevated baselines, leading to Y-intercept values > 1. This can happen when the particle size is large and concentration of sample is too low.

1.4 Factors Affecting the Hydrodynamic Radius

The factors which alter the Brownian motion or translational diffusion will invariably change the hydrodynamic radius. One of the most obvious factors is the temperature which needs to be constant throughout the experiment. Any temperature gradient will lead to convection flow, which in turn ruin the correct interpretation of the size distribution. The effect of temperature on the mean diameter of large unilamellar vesicles (can be considered as a biocolloids) is shown in Fig. 5. Viscosity is also a crucial parameter, which could change the rate of translational diffusion and hence the particle size. This is why both temperature and coefficient of viscosity appear in the Einstein-Stokes relation. Other factors that could change the hydrodynamic radius are ionic strength of the medium and shape of the particles. The fluid layer associated with the particles might be influenced by the surface structure of the particles. Therefore, the surface structure could change the diffusion speed and hence the hydrodynamic radius. Needless to say that polydispersity is an important factor in interpreting the size distribution data. We will now discuss the polydispersity of the particle and its physical significance.

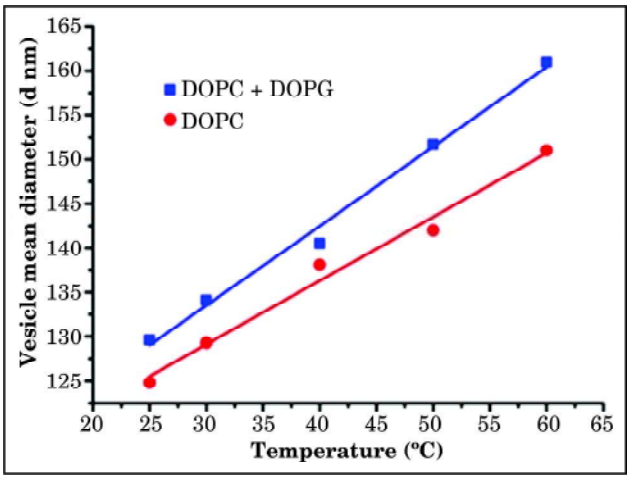

Fig. 5: Temperature dependence of large unilamellar vesicles, made from phospholipid, on the mean hydrodynamic radius.

1.5 Polydispersity

Polydispersity is a measure of dispersion or the standard deviation of size distributions. The quantitative description of polydispersity, called polydispersity index (PDI) which indicates the extent of polydispersity of distribution is defined in section 1.3. In the case of polymer chemistry, polydispersity index is defined as the ratio of weight average molecular weight to the number average molecular weight[23]. The term PDI is, therefore, often used to indicate the width of the molecular distributions of polymers[24]. However, in the context of DLS, width of the size distribution is a measure of PDI. As shown in Fig. 3c, the slope of the correlogram and width of the size distribution provide the idea of polydispersity of the sample. The cumulant analysis of correlogram described in section 1.3 gives the expression of PDI. PDI greater than 0.7 is considered to be too polydisperse to measure the size distribution. PDI<0.05 is purely monodisperse and monomodal distribution is obtained. Usually the highly monodisperse distribution is obtained only for standard sized latex polystyrene particles.

The major drawback that we encounter in DLS is the size distribution from non-spherical particles. Einstein–Stoke relation assumes the hydrodynamic radius of spherical particles only. Therefore, DLS measures equivalent spherical particles which have the same average translational diffusion as that of the non-spherical particles. It is important to mention that DLS never provide actual size of the particle as it measures only the hydrodynamic radius associated with the particle.

For accurate size information, one needs to adopt other experimental techniques, such as transmission electron microscopy. However, DLS can readily be used for several biomedical applications, such as, detecting aggregation of recombinant proteins, protein-protein, protein-RNA, protein-small molecule interactions[9] and many more. We shall now describe two specific applications where DLS is used to study interaction between molecules.

1.6 Interaction of Monovalent Ions with Unilamellar Phospholipid Vesicles

Unilamellar vesicle is an enclosed lipid bilayer shell and serves as an excellent model system of biological membranes. Here we describe the size distribution of large unilamellar vesicles (LUV) made from mixture of zwitterionic phospholipid dioleoyl phosphatidylcholine (DOPC) and negatively charged phospholipid dioleoyl phosphatidylglycerol (DOPG)[25,26]. The importance of the study of this system will be discussed later in this chapter. LUV are prepared in aqueous solvent using an extrusion technique (LiposoFast from AVESTIN (Canada) as described by Hope *et al.*[27]. Multilamellar vesicles suspension is extruded through polycarbonate membranes having pore diameters of 100 nm. This results in the formation of well defined size of LUV. This method produces vesicles of diameter ~100 nm, as measured by dynamic light scattering (Fig. 6). Size distribution of LUV containing ions was obtained at room temperature (25°C) with Zetasizer Nano ZS (Malvern Instruments, UK). The Zetasizer Nano uses 4 mW He-Ne laser of wavelength 632.8 nm.

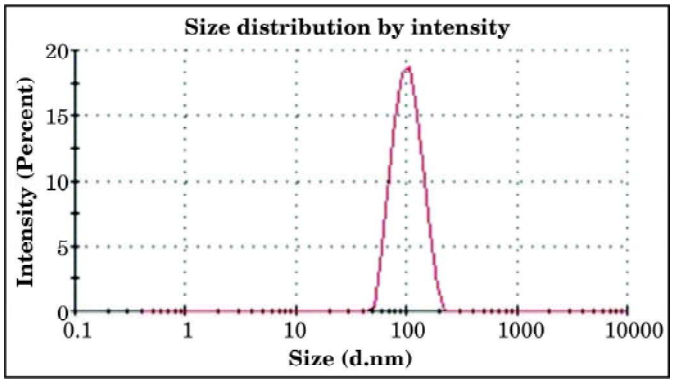

Fig. 6: Typical size distribution LUV with mean diameter 100 nm. PDI obtained from the distribution profile is 0.06 which indicates LUV are fairly monodisperse.

Various concentrations of NaCl are explored starting from 10 mM to 500 mM. The average size in terms of the effective hydrodynamic radius of LUV for different NaCl concentration is shown in Fig. 7. PDI is also presented for each salt concentration in the inset of Fig. 7. The diffusion constant is calculated from the Einstein-Stokes equation (equation 10) and is found to be $1.25 \times 10^{-12} m^2/s$ which is in agreement with the value obtained from the simulation study[28]. It is evident from the Fig. 7 that the average radius slightly decreases as the salt concentration is increased. Above 100 mM average size again increases and eventually stays constant with a value similar to that without salt concentration. The presence of ions in the medium in which negatively charged LUV are dispersed, can, in principle, alter the hydrodynamic radius by changing the thickness of the electrostatic double layer also known as Debye length. It is interesting to note that the average size of LUV decreases with the increase of salt in the intermediate concentration range. The adsorption of ions on LUV compresses the electrostatic double layer, resulting in a decrease in the hydrodynamic diameter. At a higher salt concentration >100 mM, charge screening effect overcomes the adsorption process and therefore, no more decrease in hydrodynamic radius have been observed. This result indicates the evidence of screening effect at higher concentrations of salts. Therefore DLS technique can provide us significant insight into the ion-membrane interaction.

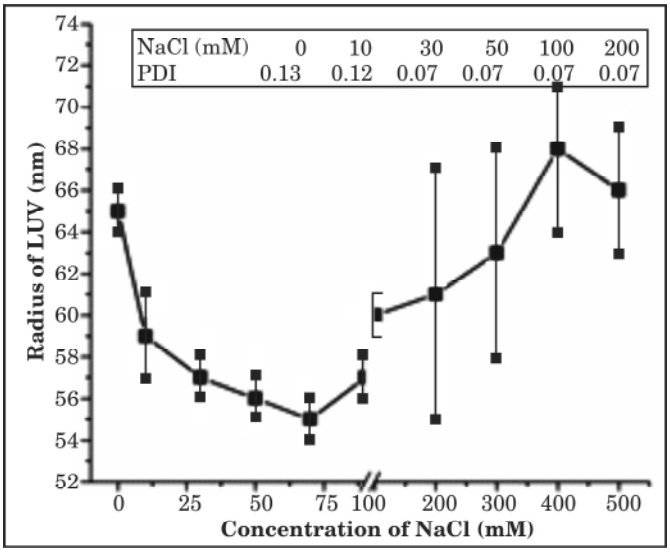

Fig. 7: The Average size (d nm) of LUV composed of DOPC-DOPG (4:1) mixture for different concentration of NaCl. Polydispersity index (PDI) is shown in the inset table. Error bars were obtained from 5 independent measurements.

1.7 Interaction of Antimicrobial Peptide with Negatively Charged Unilamellar Phospholipid Vesicles

Antimicrobial peptides (AMP) are the unique and diverse group of molecules which are part of innate immune response found in all animal and human bodies. The NK-2 is one such potent antimicrobial peptide derived from cationic core region of NK-lysin found in natural killer cells. The interaction of NK-2 with phospholipid membranes has been studied using DLS in order to get insights into the mechanisms of pore formation and membrane disruption[29]. The DLS technique can, in principle, show the evidence of membrane–membrane interaction mediated by NK-2 or the leakage of LUV induced by NK-2. DLS technique shows the evidence of strong interaction between the phospholipid membranes and the peptide. The increase in polydispersity and eventual aggregation of vesicles induced by NK-2 at higher peptide to lipid ratio is clearly seen from the correlation curve as shown in Fig. 8. In case of LUV without NK-2, PDI found in the distribution to be 0.04 which suggests that the vesicles are fairly monodisperse. The correleation curve also shows monomodal distribution which can be fitted to single exponential decay. However, in the presence of NK-2 multimodal distribution of the size arises due to strong membrane-membrane interaction induced by NK-2 which eventually leads to aggregation of vesicles. Polydispersity index found in this case is pretty large (0.9) which signifies that the sample is highly poydisperse. Signature of aggregations can also be seen from the fluctuations in the tail of the correlation curve.

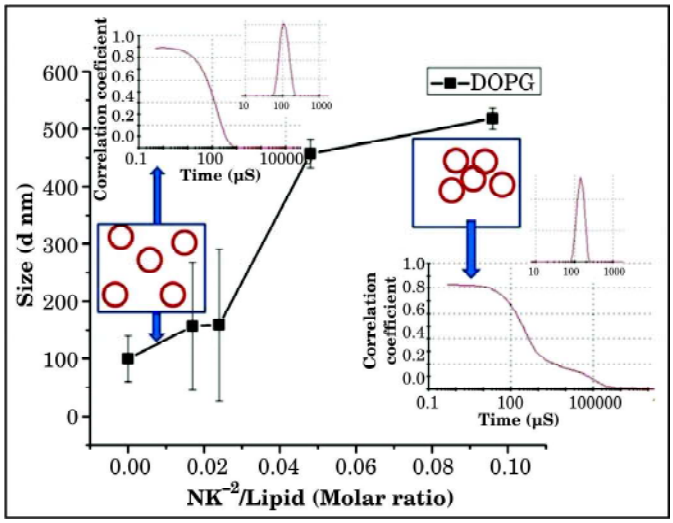

Fig. 8: Variation of average size of LUV, exposed to various concentrations of NK-2. Inset shows the correlation curve and size distributions of LUV in the presence and absence of NK-2. Schematic picture of LUV shown in the box indicates the aggregation of LUV in the presence of NK-2.

We shall now discuss another experimental technique, zeta potential measurement, based on dynamic light scattering and laser Doppler velocimetry. This technique is particularly useful and relevant for charged colloidal particles.

2. ZETA POTENTIAL

This technique is primarily being used to study the properties of particles in dispersions/emulsions and at the interfaces or biointerfaces[6]. It is used to estimate the surface charge, surface potential of the colloidal particles and to determine electrophoretic mobility, isoelectric point of charged system. Before going to the definition and significance of zeta potential, we shall discuss the electrostatic behavior of charge surface in a solvent, starting from the Poisson Boltzmann equation, for understanding the concept of zeta potential and the processes involved and to aid in manipulating the events to best advantage. The electrostatic behavior of the charged surface can be envisaged from the charged colloidal dispersion. Colloidal dispersion is a heterogeneous system formed by disperse phase and dispersion medium. Usually, one substance is dispersed as fine particles in an another substance, known as dispersion medium. Depending on the states of the dispersed phase and dispersion medium, a variety of colloidal systems are formed. In order for two phases to coexist in contact, there must be a region through which the intensive properties, such as, mechanical, electrical, optical, kinetic properties of the system change. For stability, the system must possesses an interfacial free energy such that work must be done to extend or enlarge the boundary. There exist numerous practical situations in which the energetic balance of interfacial regions must be modified in order to make use of the unique characteristics of a system[30]. For example, the presence of ions, excess electrons or inorganic group in one or both states leads to a distribution of electric charges in a nonuniform way at the interface. The stability of the system is always determined by the charge distribution at the region between two adjoining coexisting phases[31]. The importance of the charge distribution at the solid-liquid interface is manifold. The electrostatics as well as electrodynamics of charge particles in a liquid provide the basic understanding of many natural phenomena, particularly in the field of colloidal chemistry and electrochemistry. The knowledge of the distribution of charges and dipoles in the interfacial region plays vital role in understanding the mechanisms, such as, electrode kinetics, electrocatalysis, corrosion, adsorption, crystal growth, colloid stability and flow behaviour (both of colloidal suspensions and of electrolytes through porous media). Zeta potential can provide useful information

to understand a number of interesting situations and events occurring at interfaces.

A most relevant colloidal system to discuss the zeta potential is charge particles dispersed in an aqueous or a non-aqueous solvent. One such example is the dispersion of nano-sized polystyrene latex particles in an aqueous solvent. Mono-disperse small or large unilamellar vesicles made from charged phospholipids can also be an example of bio-colloids. We shall discuss the electrostatic behavior of such vesicles in details later in this chapter.

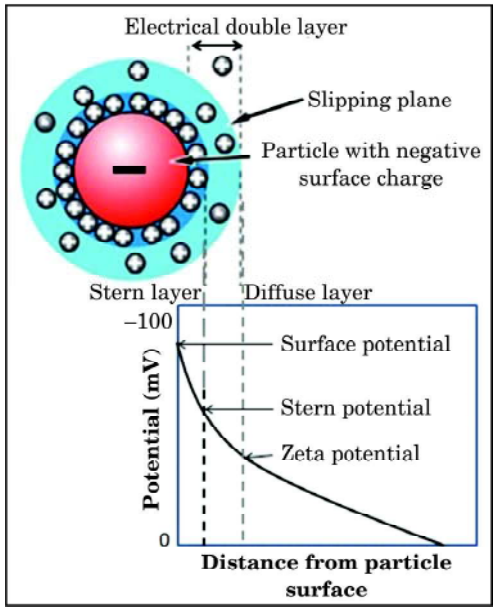

Fig. 9: Schematic representation of origin of zeta potential

2.1 Origin of Surface Charge and Stability Criteria

The van der Waal forces alone cannot determine the stability of particles in an aqueous solvent. If only attractive van der Waals forces were present, we might expect all dissolved particles to stick together (coagulate) immediately and precipitate out of solution as a mass of solid material. This does not happen to a stable dispersion of particles, as particles in the solutions acquire charges, preventing from coalescing by electrostatic repulsion. There are three different ways particles in an aqueous solvent can acquire charges[32].

(i) Ionization or dissociation of surface group. For example, the dissociation of the acid group (or basic group) on the surface of the particle leaves behind negatively (or positively) charged surface.

(ii) Adsorption or binding of ions from solution onto a previously uncharged surface. For instance, adsorption of anions (or cations) makes the zwitterionic lipid bilayer surfaces negatively (or positively) charge.

(iii) Differential loss of ions from the crystal lattice.

The magnitude of the final surface charges will depend on the strength of the acidic or basic group of the surface or the amount of ions adsorbed to the surface and the pH of the solution. Whatever the charging mechanisms, final surface charges of the co-ions will be balanced by oppositely charged counterions, as shown in Fig. 9. Usually some counterions are bound or closely associated around the oppositely charged particles and form Stern or Helmholtz layer. Other counterions close to the surface undergo rapid thermal motion and are free to diffuse. Stern layer together with a diffused layer constitute electrostatic double layer. The potential at the surface of the electrostatic double layer, also known as slipping plane, is termed as zeta potential (Fig. 9). The magnitude of the zeta potential gives an indication of the potential stability of the colloidal system. The binding affinity of counter ions with oppositely charged particles can also be estimated from the measured zeta potential. If the particles in a dispersion possess large zeta potential (> ± 30 mV, '>' is with respect to magnitude of the zeta potential and sign indicate the type of charge of particles), the strong repulsive forces prevent particles to aggregate, resulting in a stable dispersion. However, low (< ± 30 mV) zeta potential indicates unstable dispersion.

There are certain situations where particles in a dispersion may adhere and undergo a process of sedimentation, flocculation, coagulation and phase separation as described in Fig. 10. It is now necessary to discuss the responsible intermolecular forces that prevent from aggregation and keep the system stable. Four scientists Derjaguin, Landau, Verwey, and Overbeek developed a theory, known as the DLVO theory which discusses the stability of colloidal systems in terms of van der Waal attraction and electrostatic double layer repulsion[32]. At very short length scale, *i.e.*, within the few nanometer separation, contribution of interaction potential due to solvent is negligible and only van der Waal (V_A) and double layer repulsion (V_R) are important. The V_A and V_R essentially operate over a much larger distance. Dependence of these

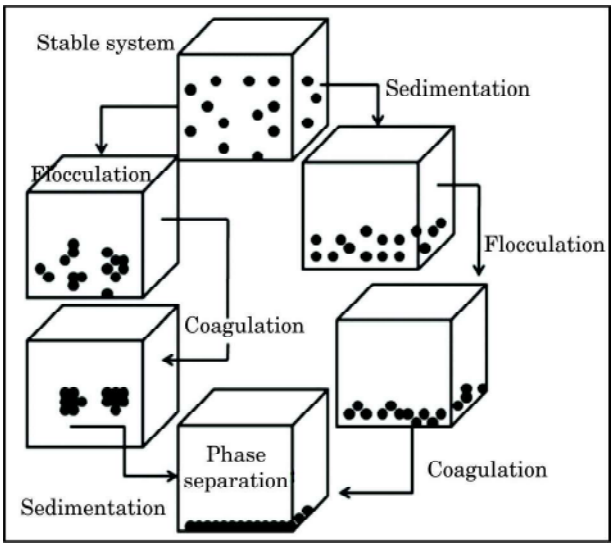

Fig. 10: Various processes that particles in a solution can undergo due to inter-particle interaction. These processes can be explained using DLVO theory.

potentials on the particle separation D is given by $V_A = -\frac{A}{12\,\pi\,D^2}$ and $V_R = 2\pi\varepsilon a\,\zeta^2\,e^{-\kappa D}$, where, A is the Hamaker constant, ε, are permeability of the medium and radius of particle, respectively. κ is the inverse Debye length, which is a function of ionic composition of the system and ζ is the zeta potential. DLVO theory suggests that the stability of colloids is determined by the competition between van der Waal attraction and double layer repulsion that exists between the particles as they approach each other due to Brownian movement. If van der Waal attraction dominates over the double layer repulsion, particles may adhere and eventually undergo flocculation. However, if particles have sufficiently high repulsive interaction to overcome the barrier of van der Waal attraction, the dispersion becomes stable. The combine effect of these two forces canbe understood clearly in Fig. 11.

Unlike electrostatic double layer interaction, van der Waal (VDW) attraction is insensitive to the electrolyte concentration in the solution and the pH. Therefore, VDW can be taken as constant over all electrolyte concentrations. Fig. 11 shows schematically both VDW and double later interaction potentials that exist between two similarly charged surfaces or colloidal particles in a 1:1 electrolyte solution.

The minimum potential energy at contact (D ~ 0) is called the primary minimum which corresponds to thermodynamically equilibrium state

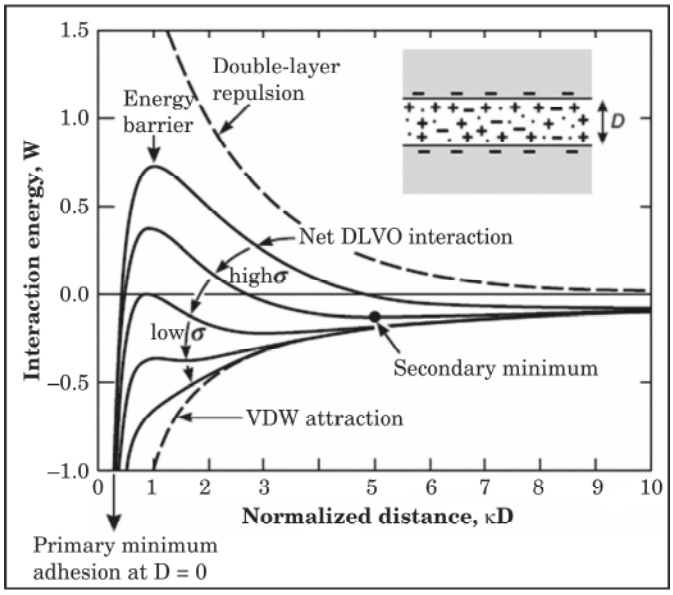

Fig. 11: Stability of colloidal suspension in a dispersant. Dashed curves indicate van der Waal (VDW) attraction and double –layer repulsion. Resultant interaction suggested by the DLVO theory is plotted as a function of charge density ó of the particles. σ can be varied by changing the electrolyte concentration in the solution[32].

for a colloidal system. For highly charged surfaces in dilute electrolyte (*i.e.*, high Σ and long Debye length), the strong long-range repulsion occurring at short distances (between 1 and 5 nm), leads to a high energy barrier (many kT). In more concentrated electrolyte solutions, a significant secondary minimum, usually beyond 3 nm, appears before the energy barrier enters into the attractive potential region. It may so happen that the energy barrier before reaching the primary minimum is so high during any reasonable time period that the particles prefer to reside either at the weaker secondary minimum or remain totally disperse in the solution. In the latter case, the colloid is referred to as being kinetically stable. The small energy barrier can be envisaged for low charge density or potential which leads to slow aggregation, known as coagulation or flocculation. However, rapid coagulation starts to happen when the energy barrier falls in the negative potential energy (Attractive regions, see Fig. 11). This happens below a certain charge or potential, or above some concentration of electrolyte, known as the critical coagulation concentration. The colloid is now referred to as being unstable. At sufficiently low surface charge or potential the interaction curve approaches the pure attractive type and two surfaces now attract each other strongly at all separations. In summary, if the electrical

double layer of a colloidal system overlap, *i.e.*, if κ^{-1} exceeds the average interparticle separation, then the system will usually be stable, given a moderate amount of charge on the particles.

This is clearly evident from the above discussions, the surface charge, potential as well as added electrolyte concentration play a crucial role in determining the stability of the colloidal dispersion. The electrostatics of particles in an aqueous solution and their stability can be obtained directly from the measurement of zeta potential which is a good approximation to a surface potential at moderate electrolyte concentration. We shall now discuss a brief theory of potential and charge distribution in the electrostatic double layer.

2.2 The Potential and Charge Distribution in Electrical Double Layer

The theory of diffused electrical double layer was first described independently by Gouy (1910) and Chapman (1913). In this model, a layer of charge is assumed to be smeared out uniformly over a plane surface immersed in an electrolyte solution. A practical example of such system is the charged membrane in an electrolyte solution. This charged surface will have electrostatic potential, called surface potential ψ_0. The compensating ions are considered as point charges embedded in a continuum dielectric medium. The charge distribution and the potential ø in this system are described by the Poisson equation.

$$\nabla^2 \psi = -\frac{\rho}{\epsilon} \tag{15}$$

Where, ε(Dielectric constant × permittivity of the free space) is the permittivity of the medium. In equilibrium, the electrical forces and the diffusive forces of the ions must balance out, *i.e.*, the electrochemical potential must be constant everywhere.

$$\nabla \mu_i = -z_i e \nabla \psi \tag{16}$$

The term in the left hand side of equation (16) describes the diffusive force of the i^{th} type of ions with valency z_i and chemical potential μ_i. The right hand side is typical electrical force, as electric field (conservative field) can be written as negative gradient of potential. For a flat electrical double layer, both the potentials are constant along the planes parallel to the wall (i.e., Ψ(y,z)= constant, considering the double layer wall is along the Y-Z plane). So equation (16) can be written in terms of one dimensional Poisson equation.

$$\frac{\partial \mu_i}{\partial x} = -z_i e \frac{\partial \psi}{\partial x} \tag{17}$$

Now the chemical potential per ions of i^{th} type is given by

$$\mu_i = \mu_0 + kT \ln n_i \tag{18}$$

where n_i is the number of ions of i^{th} type per unit volume. From eqs. (17 and 18) we get

$$\frac{d \ln n_i}{dx} = \frac{1}{n_i}\frac{dn_i}{dx} = -\frac{1}{kT} z_i e \frac{\partial \psi}{\partial x} \tag{19}$$

Solution of equation (19) with a boundary condition that $\psi = 0$ at bulk, *i.e.*, $n_i = n_i^0$. Where n_i^0 is number density of ions of a particular type i at bulk. Therefore, Boltzmann distribution of each type of ion is given by

$$n_i = n_i^0 \exp(-z_i e\psi/kT) \tag{20}$$

Equation (20) gives the local concentration each type of ion in the vicinity of the double layer region, provided the correct sign of z_i is taken in the equation. For positive ions $z_i = +ve$ and $n_i < n_i^0$ and for negative ion $n_i > n_i^0$. Volume charge density near the charged surface is given by

$$\rho = \sum_i n_i z_i e \tag{21}$$

where the summation is over all species of ions present in the solution. Using equation (20) in equation (21) we get $\rho = \sum_i n_i z_i e = \sum_i n_i^0 z_i\, e \exp(-z_i e\psi/kT)$. Now equation (15) in one dimension be written as

$$\frac{\partial^2 \psi(x)}{\partial x^2} = -\frac{\rho}{\epsilon} = -\frac{1}{\epsilon}\sum_i n_i^0 z_i\, e \exp(-z_i e\psi/kT) \tag{22}$$

Equation (22) is a non linear second order differential equation and can be solved analytically as well as numerically. Let us now examine an approximate solution for the electrical energy associated with double layer which is much smaller than thermal energy, i.e., $z_i e\psi \ll kT$. This approximation is known as Debye-Hückel approximation. Therefore,

the argument of the exponential term is small and can be expanded using Taylor series ($e^{-x} \approx 1 - x$) keeping only the linear term.

$$\frac{\partial^2\psi(x)}{\partial x^2} = \frac{1}{\epsilon}\sum\nolimits_i (n_i^0 z_i\, e + z_i{}^2 e^2 n_i^0\, \psi/kT) \tag{23}$$

The 1st term in the right hand side of the equation (22) is zero, in order to preserve the electroneutrality in the bulk. Therefore, equation (22) can be written as

$$\frac{\partial^2\psi(x)}{\partial x^2} = \kappa^2\psi \tag{24}$$

Where $\kappa^2 = \frac{e^2}{\epsilon kT}\sum\nolimits_i z_i{}^2 n_i^o$. The parameter $\kappa = \left(\frac{e^2 \sum_i z_i{}^2 n_i^o}{\epsilon kT}\right)^{1/2}$, known as Debye-Hückel parameter or inverse Debye length, is a function of electrolyte concentration and has a great significance in colloid science. To solve equation (24) to obtain $\psi(x)$ as a function of x, multiply equation (24) by $2\frac{\partial\psi}{\partial x}$ and integrating the entire equation.

$$\int 2\,\frac{\partial\psi}{\partial x}\frac{\partial^2\psi(x)}{\partial x^2}dx = \int 2\,\frac{\partial\psi}{\partial x}\kappa^2\psi$$

$$Or \int \frac{d}{dx}\left(\frac{d\psi}{dx}\right)^2 dx = \int 2\kappa^2\psi d\psi (\text{for } x = \infty, \psi = 0) \tag{25}$$

$$\text{Or, } \frac{d\psi}{dx} = -\kappa\psi \tag{26}$$

The negative sign is chosen when Ψ is positive and decreases to zero at the bulk solution. The solution of the equation (26) gives

$$\psi(x) = \psi_0 \exp(-\kappa x) \tag{27}$$

The exponential decay, as given in equation 27, is not applicable to many colloidal systems near the surface of the electrical double layer. Therefore, we need to seek for a general solution of equation (22).

$$\int d\left(\frac{d\psi}{dx}\right)^2 dx = -\frac{2}{\epsilon}\int \sum_i n_i^0 z_i\, e \exp\left(-\frac{z_i e\psi}{kT}\right) d\psi$$

$$\text{or,} \left(\frac{d\psi}{dx}\right)^2 = \frac{2kT}{\epsilon}\sum n_i^0\ \left[\exp\left(-\frac{z_i e\psi}{kT}\right) - 1\right] \tag{28}$$

As the charge distribution is symmetric for most electrolytes, the number of ions is exactly same as the number of counter ions which adsorb in the form of electrical double layer. Equation (22) turns out to be

$$\frac{\partial^2\psi(x)}{\partial x^2} = \frac{2n_0\, ze}{\epsilon}\sinh(ze\psi/kT) \tag{29}$$

Where $n_0 = n_+^0 = n_-^0$ and $z_+ = -z_-$

$$\left(\frac{d\psi}{dx}\right)^2 = \frac{4n_0kT}{\epsilon}\left(\cosh\frac{ze\psi}{kT} - 1\right)$$

$$\frac{d\psi}{dx} = -(8n_0kT/\epsilon)^{1/2}\sinh ze\psi/kT \tag{30}$$

$$\text{or}\frac{d\psi}{dx} = -\frac{2\kappa kT}{ze}\sinh ze\psi/2kT \tag{31}$$

Again the negative sign indicates that ψ falls to zero at a distance far from the wall. Solution of equation (30) can be obtained by integrating the equation and expressed in the following form

$$\tanh\frac{ze\psi}{4kT} = \tanh\frac{ze\psi_0}{4kT}\exp(-\kappa x) \tag{32}$$

For small values of p, $\sinh p \approx \tanh p \approx p$. In this case equation 31 reduces to 27. The approximate formula is always an overestimate of the potential. Far from the electrical double layer one assumes $p\ (= \frac{ze\psi}{4kT})$ is small and $\tanh p \approx p$ and equation (32) reduces to

$$\frac{ze\psi}{4kT} = \tanh\frac{ze\psi_0}{4kT}\exp(-\kappa x) \tag{33}$$

$$\psi = \frac{4kT}{ze}\gamma\exp(-\kappa x) \tag{34}$$

$$\text{here, } \gamma = \tanh\frac{ze\psi_0}{4kT} = \frac{\exp\left(\frac{ze\psi_0}{2kT}\right)-1}{\exp\left(\frac{ze\psi_0}{2kT}\right)+1} \tag{35}$$

The γ approaches unity for high values of $\frac{ze\psi_0}{kT}$. One expects the potential far from the surface to become $\frac{4kT}{ze}$ provided the surface potential is sufficiently high. Typical value of such potential ~ 100 mV/

z. The equations (27), (32) and (33) describe the behavior of electrostatic potential from the wall of the charged surface. The effect of electrolyte concentration appears through the parameter κ which is the measure of thickness of electrical double layer. Putting values of all parameters sin expression of κ, it can be written as $\kappa = 3.288\sqrt{C_{ion}}$ nm^{-1}. C_{ion} is the molar concentration of ions. κ Increases with increasing concentration of ions (see Fig. 12). As a result the potential from the charged surface falls rapidly as shown in Fig. 12. As $\frac{1}{\kappa}$ measures the thickness of the double layer, the compression of double layer occurs as is increased. The decrease in LUV radius with increasing NaCl concentration, as presented in Fig. 7 might be the consequence of the compression of electrical double layer. We shall discuss the zeta potential study of the LUV later.

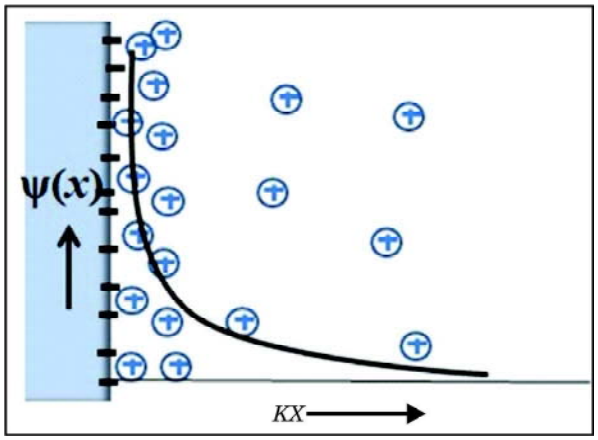

Fig. 12: Variation of potential obtained from the Gouy Chapman theory.

2.3 Surface Charge Density

The surface charge density (σ_0), *i.e.*, amount of charge per unit area can be determined from the following equation

$$\sigma_0 = \int_0^\infty \rho dx = \epsilon \int_0^\infty \frac{d^2\psi}{dx^2} = -\epsilon \left(\frac{d\psi}{dx}\right) \text{ at } x = 0 \qquad (36)$$

For symmetrical electrolyte solution, equation 35 can be written using equation 27

$$\sigma_0 = \left(2\epsilon kT \sum n_i^0 \left[\exp\left(-\frac{z_i e\psi}{kT}\right) - 1\right]\right)^{1/2}$$

However, for symmetrical electrolyte

$\sigma_0 = \frac{4n^0 ze}{\kappa} \sinh ze\psi/2kT = 11.74\sqrt{C_{ion}} \sinh(19.46z\psi_0)$ μC cm^{-2}. Here ψ_0 is in volt and C_{ion} is mole/litre. For very small potential, we can use equation (26) to obtain σ_0 as

$$\sigma_0 = \epsilon\kappa\psi_0 \tag{37}$$

From equation (36) it is evident that this system behaves like a parallel plate capacitance with separation of $\frac{1}{\kappa}$ between the two plates.

When charged particles move through the liquid under the action of an electric field, three distinct electrokinetic effects depending on the way the motion is induced come into the picture. These effects are electrophoresis, electroosmosis and streaming potential. Zeta potential is measured from the electrophoresis experiment. Before describing the experiments, let us discuss the phenomenon of electrophoresis and the working formula to determine zeta potential. Later we shall also describe how electroosmosis affects the measurement of electrophoresis.

2.4. Electrophoresis

The movement of charged particles suspended in solution towards the oppositely charged electrode when an electric field is applied across an electrolyte solution is known as electrophoresis. The force acting on the particles due to the application of electric field is known as the electrophoretic force. The velocity of a particle in a unit electric field is referred to as its electrophoretic mobility μ. Zeta potential is related to the electrophoretic mobility by the Henry equation (32).

$$\zeta = \frac{3\mu\eta}{2\epsilon f(\kappa a)} \tag{38}$$

where η and ε are coefficient of viscosity and permittivity of the aqueous medium, respectively. The Henry function, $f(\kappa a)$ depends on the inverse Debye length (κ) and the radius of the particle a. Now, κ can be defined as

$$\kappa = \sqrt{\frac{2e^2 C_{ion}}{\epsilon kT}} \tag{39}$$

where, e is the electronic charge, k is the Boltzmann constant, and T is the temperature. C_{ion} is the concentration of electrolyte in the solution. $f(\kappa a)$ was estimated using the following equation.

$$f(\kappa a) = \begin{cases} 1 & \text{for } \kappa a < 1 \\ \frac{1}{6}\ln(\kappa a) + 1 & \text{for } 1 < \kappa a < 1000 \\ 1.5 & \text{for } \kappa a > 1000 \end{cases} \quad (40)$$

The Debye length, (κ^{-1}) is often taken as a measure of the "thickness" of the electrical double layer (Fig. 13a). Typical variation of Debye length and Henry function $f(\kappa a)$for a particle of diameter ~ 100 nm dispersed in a various salt concentration, estimated from equations (39 and 40), are shown in Fig. 13b. The argument of the Henry function, *κa,* measures the ratio of the particle radius to electrical double layer thickness. For moderate electrolyte concentration, electrophoretic mobility and zeta potential are most commonly measured in aqueous media and with $f(\kappa a) = 1.5$ which is known as the Smoluchowski approximation. For small particles in low dielectric constant media *f(κa)* becomes 1.0 which is referred to as the Hückel approximation. Particles in a non-aqueous solvent generally use Hückel approximation. The corrected zeta potential is obtained by putting the modified Henry function into the eq. (38). Effective charge, Q_{eff}, of the particle can also be estimated from the measured electrophoretic mobility according to equation (41), where a_{eff} is the effective radius of the particle, including stern layer and can be obtained from DLS.

$$\mu = \frac{Q_{eff}}{6\pi\eta a_{eff}} \quad (41)$$

2.5. Determination of Electrophoretic Mobility from Dynamic Light Scattering

The electrophoretic mobility of the particle is measured from the scattering of light from particles that move in liquid under the influence of an applied electric field. The basic technique is known as Laser Doppler velocimetry (LDV) or electrophoretic light scattering (ELS). The charged particles moving under the influence of the electric field E will attain the terminal velocity v which is proportional to E.

$$v = \mu E \quad (42)$$

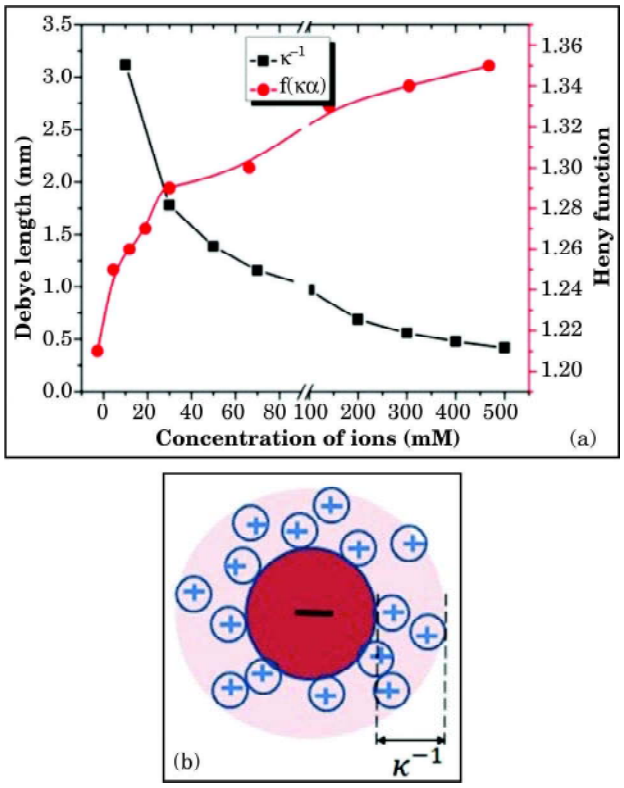

Figs. 13: Schematic picture of electrostatic double layer (a) Variation of Debye length and Henry function $f(\kappa a)$ for a particle of radius ~100 nm dispersed in a various salt concentration (b)[26].

When light of frequency (ν_i) and wavelength λ is incident on a moving particle in an applied electric field, the scattered light will undergo a Doppler shift in frequency, $\Delta\nu$, as depicted in Fig. 14. The amount of Doppler shift depends on the velocity of the particle, the wavelength of the light in the medium and the scattering angle θ and can be expressed as $2\pi\Delta\nu = q.\nu$, where q is the scattering vector defined in Fig. 2.

Now,

$$\Delta\nu = \frac{q.v}{2\pi} = \frac{4\pi\, n \sin\theta}{2\pi\lambda}\, v\, \cos\theta = \frac{v\, n \sin 2\theta}{\lambda} \tag{43}$$

Where n is the refractive index of the liquid medium. From equations (42 and 43) we obtain

$$\mu = \frac{v}{E} = \frac{\lambda\Delta\nu}{n\, E \sin 2\theta} \tag{44}$$

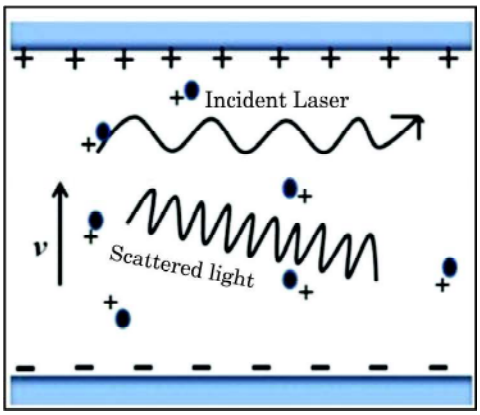

Fig. 14: Schematic diagram of scattering by moving particles under the influence of electric field showing the frequency shift in scattered light.

Equation (43) shows that $\Delta\nu$ is directly proportional to the particle velocity ν. Therefore, the determination of electrophoretic mobility μ requires the accurate measurement of $\Delta\nu$. Finally, the value of the mean zeta potential, ζ, is obtained from the μ using equation (38). The factor 3/2 appears in the expression due to Hückel limit. In this limit $\kappa a \ll 1$ and Debye length overlaps with the interparticle separation. Now we are ready to discuss detailed experimental method to obtain μ.

2.6. Measurement of Electrophoretic Mobility

A typical experimental geometry to measure μ in a scattering experiment is shown in Fig. 15. A classical micro-electrophoresis system consists of a cell with electrodes at either end to which a potential is applied. Particles move towards the electrode of opposite charge, their velocity is measured and expressed in unit field strength as their mobility. A laser is used to illuminate the sample after it has passed through a beam splitter. The beam splitter produces a reference beam which will later interfere with the scattered beam. The velocity of the particles undergoing electrophoresis is determined by comparing the beat frequency detected with that of a reference frequency. The scattered beam is usually detected at a small angle typically 10 to 15°. The resulting coherent superposition between reference beam and the scattered beam is transmitted to the detector (Usually photo detector, such as PMT or APD) by the optical fiber. In order to enhance the Doppler shift the reference beam is also modulated with an oscillating mirror before it combines with the scattered beam to improve signal to noise ratio. The mobility of the particles in an applied field will therefore produce a

frequency shift away from that of the modulator frequency. All that is required to determine $\Delta\mu$ is to measure the frequency power spectrum of the detector output signal. Detector sends the information to a digital signal processor. Proper design and synchronization of the electronic waveforms that drive the cell electrode voltage and optical modulator allow the sign, as well as the magnitude, of the frequency shift to be determined.

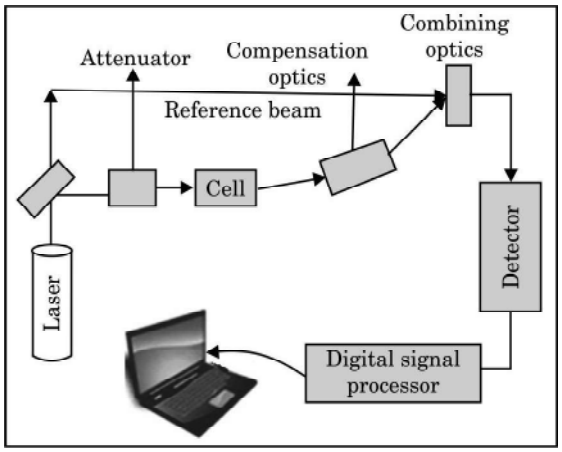

Fig. 15: Schematic experimental geometry for the measurement of zeta potential

The electroosmosis within the sample capillary cell will affect the electrophoresis process. Electroosmosis is the movement of a liquid relative to stationary charged surface. In order to avoid electroosmosis, phase analysis light scattering (PALS) technique is adopted. PALS is a technique that uses the same optical setup as conventional laser Doppler electrophoresis. However, a different signal processing method is employed. PALS measures the phase (frequency × time) shift between scattered light and reference beam instead of frequency shift. The detection of phase change is more sensitive to changes in mobility than the traditional detection of frequency shift. Details of this technique and its consequence in the context of electrophoresis measurement are discussed elsewhere[15,33]. Here we discuss briefly the PALS technique to measure phase shift.

The phase shift in the scattered light is proportional to the change in the position of the particles. A reasonable contribution of electrophoretic mobility to the particle motion can be obtained by sampling many oscillations of frequency shifted signals (Fig. 16a). For high mobility particles, enough data can be produced within the measurement time for accurate determination of particle motion. This is true as high mobility

particles pick up a lot of energy from the electric field and move quickly. However, the effect of electric field on low mobility particles is too weak to produce enough data and often a fraction of oscillation can be obtained within the measurement time (Fig. 16b). In such case, electrophoretic mobility would not be possible to determine from standard Fourier transform analysis. Therefore, the strength of the applied electric field to the sample needs to be increased in order to compensate the electric field. However, the increase in the strength of the applied electric field, especially for high conductivity sample, leads to significant Joule heating which affects the random motion of particles and can denature the sample. Now a small change in frequency leads to a considerable large change in phase between beat frequency and the reference frequency. By measuring the phase differences, the changes of the position of the particle can be determined more accurately. When the phase difference between two signals (Figs. 16c-d) of different frequencies is plotted over time (Fig. 16e), a gradient line is obtained. The PLAS measures the slop

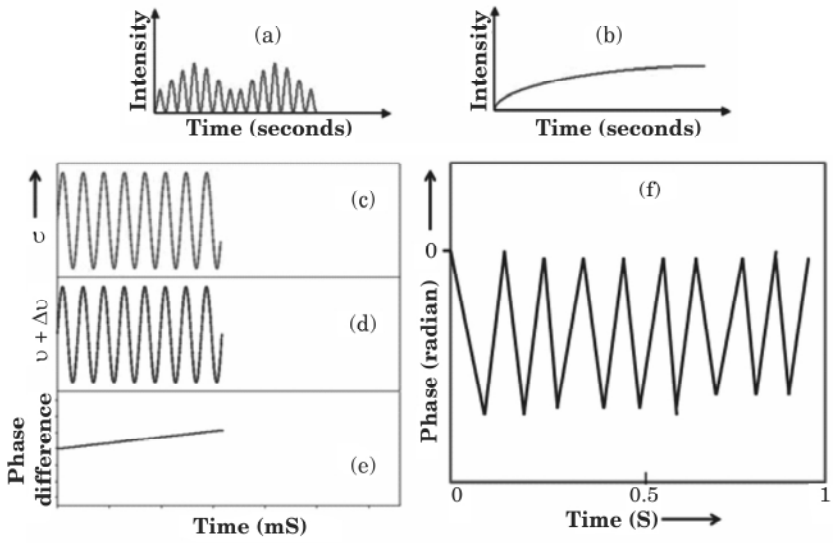

Fig. 16: (a) For high mobility particles, enough data is collected within the measurement time to produce an accurate determination of the particle motion; (b) For low mobility particles, only a fraction of an oscillation may have been completed within the measurement time. Schematic diagram showing the phase difference between two signalsl; (c–d) of two different frequencies ν and ν + Δν. Plot of phase difference between two signals , depicted in (c–d) with time shows straight line; (e) Slop or gradient of the line determines the velocity of particles and the electrophoretic mobility; (f) is the typical phase plot with time which is obtained due several times field reversal during the measurement sequence.

of the line, *i.e.*, the rate of change of phase difference which is related to the velocity of the particles. By measuring the velocity of the particles, the zeta potential can be determined. Fig. 16f shows typical phase plot that is obtained from the zeta potential measurement. The well-defined alternating slopes of the phase difference with time that, are obtained due to number of times rapid reversal of applied filed during the measurement sequence. These slopes are averaged to determine the mean phase difference and hence mean zeta potential.

There are several major advantages of PALS techniques over standard measurement techniques. PLAS allows to measure high conductivity sample at moderately low electric field to avoid the risk of sample effect such as joule heating. Besides this, the low electric field also prevents the electrolysis of the sample which might damage the electrodes of the sample cell. It is also useful for low mobility particles *i.e.*, high viscosity and non aqueous applications. In a typical experiment each measurement of zeta potential consists of several runs to minimize the statistical errors. The typical output from the instrument (Malvern zetasizer nano ZS) is shown as Fig. 17. In addition to the distribution

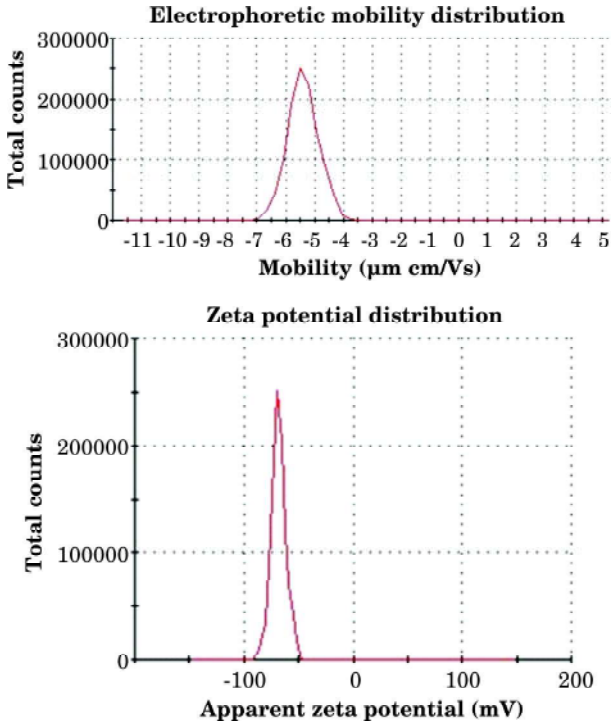

Fig. 17: Typical electrophoretic mobility and zeta potential distributions obtained from a standard sample.

profile, measurement will also provide data for frequency shift and phase plot of the signal.

2.7. Factors Affecting Zeta Potential

The most important factor that affects zeta potential is pH. As pH of the solution changes the effective charge state of the particles, zeta potential value also changes. Therefore, zeta potential value without mentioning the pH is meaningless. Fig. 18 shows the zeta potential at different pH. The variation zeta potential with pH also enables us to determine the isoelectric point (IEP) as indicated in Fig. 18. It is the point at which the particles do not possess net charges. For example, if more alkali is added to the particle suspension with negative zeta potential, then the particles tend to acquire a more negative charge. Alternatively, if acid is added to this suspension, the zeta potential will approach towards positive value and eventually a point will be reached where the charge will be neutralized. This point is called the IEP. Further addition of acid will cause a buildup of positive charge, as depicted in the positive zeta potential in Fig. 18. The IEP is indeed an important practical consideration for many applications, especially in the field of colloid science and biochemistry. For example, IEP is used for detection and prevention of protein aggregation before, during, and after purification[34,35]. It is normally the point where the colloidal system is least stable[36].

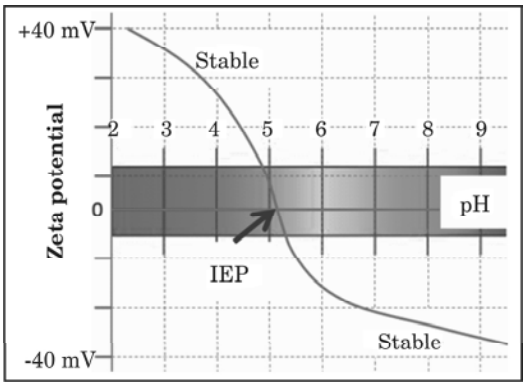

Fig. 18: Dependence of zeta potential on pH of the solution. The point indicates by IEP is the isoelectric point[37].

As discussed before (Fig. 13), the thickness of the double layer (κ^{-1}) can be estimated from the ionic strength of the medium. The double layer becomes more compressed, as seen from decreasing the value of κ^{-1} at higher ionic strength. The extent of decrease in κ^{-1} also depends

upon the valency of the ions. Higher valency, such Ca^{+2} or Al^{+3} will compress the double layer to a greater extent than that of monovalent ions, such as Na^{+}. The specific adsorption of ions onto a particle surface, even at low concentrations, can have a dramatic effect on the zeta potential of the particle dispersion. We shall discuss later this aspect with an example of peptide adsorption onto negatively charged vesicles. High ionic strength typically more than 500 mM concentrations of ions affects zeta potential significantly. High ionic conductivity is not suitable for the measurement which may lead to electrolysis of the electrode. Therefore, at high ionic strength, the electrode may get damaged. The best result we could get is for moderate electrolyte concentration[25]. Now we shall discuss two specific examples for the measurement of zeta potential. These systems are already discussed in the context of size measurement using dynamic light scattering.

2.8. Zeta Potential of Unilamellar Vesicles Prepared from Charged Phospholipids

The effect of various types of ions on model membranes has enticed significant interest due to their immense biological applications[38]. For example, trans-membrane potential may arise from the asymmetric binding of Na^{+} and Cl^{-} ions which in turn affect ion transport across the bilayer[39]. In 1888, Hofmeister proposed a series which qualitatively arranged ions according to their propensity to precipitate proteins[40]. The presence of ions in the aqueous medium plays a vital role in modulating bilayer properties. Electrostatics of the ion-membrane interaction can be best described by measuring zeta potential[41]. As discussed before, zeta potential is a potential at the electrical double layer and can be used to determine surface charge distributions using Gouy Chapman theory. Therefore, the affinity of ions towards the charged membrane and hence the binding constant of ions is determined[25,26,42]. The Fig. 19 shows the result of zeta potential of LUV composed of negatively charged lipids (already mentioned before) for various alkali metal ions. The affinity of these ions with the negatively charged membranes are inferred from the zeta potential and the order of affinity is presented at the top of the figure 19. The formation of electrical double layer around the LUV is also depicted in the Fig. 19.

As evidenced from Fig. 19, Li^{+} and Na^{+} ions show stronger adsorption affinity relative to other alkali metal ions. In summary, the affinity of ion adsorption to negatively charged membranes follows the sequence Li^{+}> Na^{+}> K^{+}> Cs^{+}>Rb^{+} which is consistent with the Hofmeister series. As expected, zeta potential increases with increasing ion concentration. Measurement of zeta potential from electrophoretic mobility also becomes

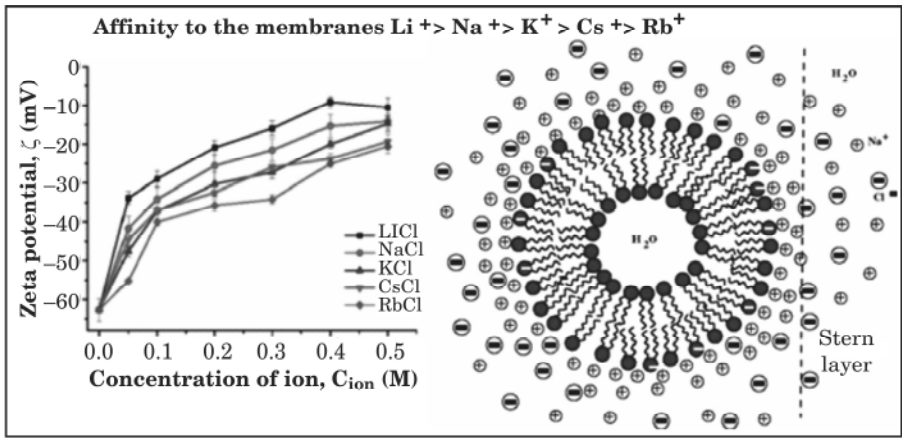

Fig. 19: Effect of various monovalent alkali metal ions with negatively charged phospholipid vesicles composed of DOPC-DOPG (4:1).

difficult at high salt concentration, as this may damage the gold electrodes of the zeta cuvette. The behaviour of zeta potential for three different lipid compositions is shown in Fig. 20. LUV, made from a neutral lipid (DOPC), show zeta value close to zero, indicating very low ion adsorption affinity. It is expected for neutral membranes as the zeta potential can only be realized with respect to the charged membranes. However, the zeta potential increases significantly in the case of negatively charged LUV, indicating higher adsorption affinity of cations towards negatively charged lipid than of that neutral lipid. We shall now briefly describe how Gouy Chapman theory is used to determine the binding constant of alkali metal ions in 1:1 electrolyte.

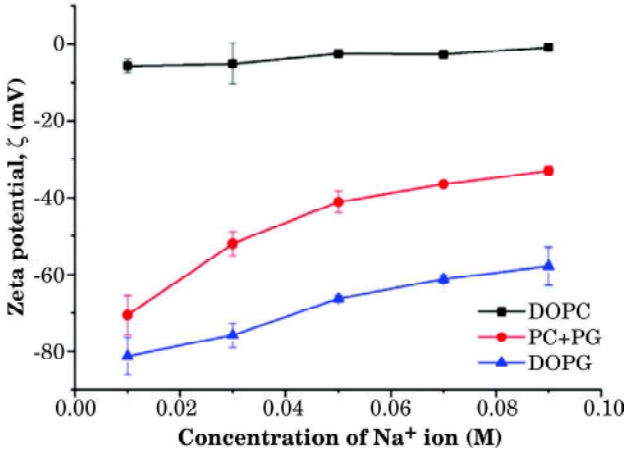

Fig. 20: Variation of zeta potential with different concentration of NaCl for three different phospholipid vesicles, indicated in the figure[25].

2.9. Electrostatics of Charged Membranes

The binding constant essentially measures the relative ratio of number of ions that bind to the membranes to the number of free ions present in the bulk. Total ion concentration in the solution is the sum of bound ions and free ions. Therefore, the apparent binding constant is usually obtained in many experimental techniques, such as isothermal titration calorimetry and fluorescence spectroscopy techniques. The apparent binding constant K_{app} is defined as $X_b = K_{app} C_f$, where X_b is the extent of ion binding per mole of lipid and C_f is the free ion concentration of the solution. When the ions adsorb, the membrane becomes charged. Hence, further adsorption of ions onto the membrane is restricted by electrostatic repulsion. Therefore, K_{app} is no longer a constant, but rather changes with C_f. Therefore, the most relevant binding parameter would be the intrinsic binding constant K_{int} which is assumed to be directly proportional to the concentration of ions (C_M) at the vicinity of the membrane surface. The binding model essentially calculates X_b and C_M using Gouy Chapman theory as described before. The surface concentration C_M of monovalent cations at the vicinity of the membrane solution interface, is described by the Boltzmann relation (also see equation 20).

$$C_M = C_B \exp\left(\frac{-Ze\psi_0}{kT}\right) \tag{44}$$

Where C_B is the bulk concentration of the cations. The surface charge density σ is estimated from the Gouy Chapman theory. The theory assumes that charges are located on the surface of the membranes and are smeared uniformly over the entire surface. The zeta potential (ζ) is defined as the potential at the shear plane or diffused layer. The hydrodynamic plane of the shear is assumed to be located at a distance x=2 Å from the charged surface of the membranes[42]. From the knowledge of zeta potential, *i.e.*, ψ(x= 2 Å)=ζ, the surface potential ψ_0 was calculated. The adsorption of monovalent ions onto the membrane alters the surface charge density (σ) and σ for each electrolyte concentration can be obtained from the Gouy–Chapman relation discussed the section 2.3.

Langmuir adsorption isotherm describes the simplest approach to the binding of cations with the charged lipids, which relates to the surface charge density with K_{int} from the knowledge that the maximum charge density of the membrane in the absence of ions σ_0 (~1.4×10^{14} charges per $cm^2 \equiv$ "0.228 C/m^2)[43] and C_M.

$$\sigma = \frac{\sigma_0}{1 + K_{int} C_M} \tag{45}$$

Therefore, using equation (45), the intrinsic binding constant can be estimated. Results from the Gouy Chapman theory is presented in Table 2.

Table 2: Binding parameters obtained from the zeta potential for a 100 mM salt concentration[25].

Alkali metal ions	*Zeta potential (mV)*	*Surface potential ψ_0 mV)*	*Surface charge σ (C/m^2)*	*Surface concentration C_M (mM)*	*Intrinsic binding constant $K_{int}(M^1)$*
Li^+	–29 ± 2	–36 ± 2	–0.028 ± 0.002	410 ± 40	1.4 ± 0.9
Na^+	–34 ± 3	–43 ± 4	–0.034 ± 0.003	520 ± 80	0.6 ± 0.2
K^+	–37 ± 1	–47 ± 2	–0.039 ± 0.002	620 ± 40	0.3 ± 0.1
Cs^+	–37 ± 2	–47 ± 1	–0.039 ± 0.001	620 ± 10	0.3 ± 0.1
Rb^+	40 ± 1	–51 ± 1	–0.043 ± 0.001	720 ± 10	0.1 ± 0.1

The ideal concentration range that one should use to study the binding phenomena of ions with the membranes is 10-100 mM. It is interesting to note that even at moderate concentration of salts, the intrinsic binding constant decreases with increasing salt concentrations[25]. The surface potential as well as zeta potential are determined by the competition between the binding of ions and charge screening effect. As the Debye screening length decreases very rapidly with concentration, charge screening effect increases with increasing concentration of ions and eventually overcomes the binding of cations. This might be the reason why higher concentrations of salt (> 200 mM) are not suitable for analysis of binding phenomena from the measurement of zeta potential.

2.10 Interaction of Antimicrobial Peptide NK-2 with Various Phospholipid Membranes: Zeta Potential Study

The interaction of NK-2 with negatively charged membranes has already been illustrated in terms of size distribution obtained from DLS (see section 1.6). Zeta potential was measured in LUV composed of different lipids or lipid mixtures for various concentrations of NK-2. Results are presented in Fig. 21[29]. It is clearly evident from Fig. 21 that the zeta potential increases significantly with increasing NK-2 to lipid molar ratio (NK-2/L) for all charged LUV. Although phospholipids such as DOPC and a mixture of DOPC-DOPE are neutral, they exhibit low negative value and increase to a positive zeta potential due to adsorption of peptide onto the membrane surface. As NK-2 possesses high (+10 in

pH 7.4) positive charge, the charge compensation occurs at different NK-2/L for different lipid mixtures. The overcharge compensation occurs at a different NK-2/Lipids ratio for all different lipid compositions which indicates the entropic contribution besides the electrostatic interaction between charged membrane and the peptide. The modified Gouy Chapman equation can be used to estimate the intrinsic binding constant of NK-2 with phospholipid membranes.

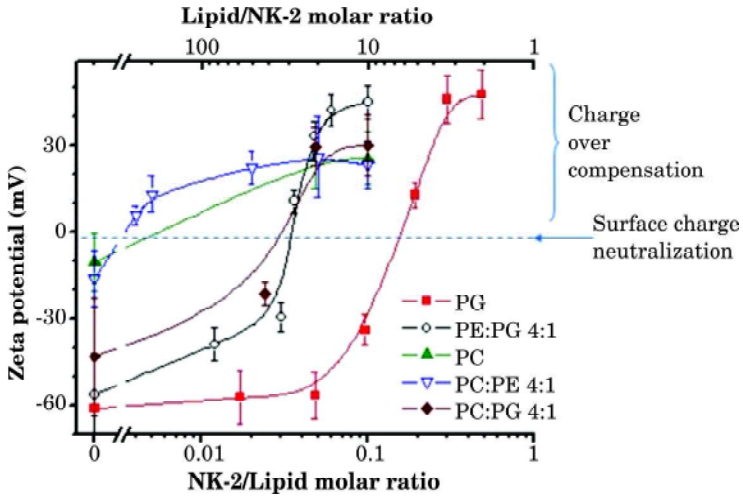

Fig. 21: Zeta potential of phospholipid LUV at various NK-2 to Lipids molar ratio. Solid lines are intended only as guides to the points. Error bars indicate the width of the distribution profile of zeta potential[29]

It is important to mention that change in the size distribution of vesicles does not influence the zeta potential significantly. Zeta potential is estimated from the Smoluchowski approximation, where the Henry function $f(\kappa a)$ takes its maximum value 1.5. In other words, zeta potential is determined from the electrostatic double layer formation which does not depend on the size of the particle.

Apart from size distribution and zeta potential measurements, DLS can also be used to measure rheological properties of a fluid by measuring the scattered intensity from tracer particles embedded in the solution. Dynamic light scattering microrheology is a passive characterization technique that uses tracer particle and probes linear viscoelastic properties, such as viscosity and viscoelastic moduli of low viscosity and weakly structured fluids.

To conclude, we discuss two important non-invasive experimental characterizations namely particle size distribution and zeta potential

based on dynamic light scattering along with laser Doppler velocimetry. These characterizations are widely and routinely used in many interdisciplinary fields of science including nanotechnology. In order to interpret and explain the experimental results obtained from DLS and zeta potential, it is necessary to understand the techniques as well as theory behind. In the present chapter, we intend to provide some details of DLS techniques and underlying theory.

ACKNOWLEDGMENTS

The author sincerely acknowledges the Department of Biotechnology (DBT), Govt. of India (BT/PR8475/BRB/10/1248/2013).

BIBLIOGRAPHY

[1] Berne, B.J. and Pecora. R. (2000). Dynamic Light Scattering: With Applications to Chemistry, Biology, and Physics. New York: Dover Publications. Inc.
[2] Tyndall, J. (1868). On the blue colour of the sky, the polarization of skylight, and on the polarization of light by cloudy matter generally. *Proc. Royal Soc. Lond*, 17: 223–233.
[3] Hergert, W. and Wriedt, T. (*eds.*) (2012). *The Mie Theory: Baiscs and Applications.* Springer, 2012.
[4] Yeh, C. and Lee, W.C. (1978). Rayleigh-Debye scattering with focused laser beams. *Appl. Optics*, 17: 1637–1643.
[5] Pecora, R. (*ed.*) (2011). Dynamic light scattering: Applications of photon correlation spectroscopy. Spinger.
[6] Hunter, R. (1981). Zeta Potential in Colloids Science: Principles and Applications. Ottewill, R.L. and Rowell, R.H. (*ed.*), New York: Academic Press.
[7] Guinier, A. X-Ray Diffraction In Crystal, Imperfect Crystals, and Amorphous Bodies. W.H. Freeman and Company, San Francisco and London.
[8] Bhattacharjee, S. (2016). DLS and zeta potential – What they are and what they are not? *J. Control. Release*, 235: 337–351.
[9] Stetefeld, J., McKenna, S.A. and Patel, T.R. (2016). Dynamic light scattering: a practical guide and applications in biomedical sciences. *Biophys. Rev.*, 8: 409–427.
[10] Smoluchowski, M. (1906). Essai d'une théorie cinétique du mouvement Brownien et des milieux troubles (Outline of the kinetic theory of Brownian motion of suspensions. Bulletin International de l'Académie des Sciences de Cracovie. pp. 577–602.
[11] Einstein, A. (1906). Zur Theorie der Brownschen Bewegung. *Annalen Der Physik*, 324: 371–381.
[12] Beale, P.D. and Pathria, R.K. (2011). Statistical Mechnics. 3rd ed., Elsevier Ltd.
[13] *https://www.lsinstruments.ch/technology/dynamic_light_scattering_dls/.*
[14] *http://www.horiba.com/scientific/products/particle-characterization/technology/dynamic-light-scattering/.*
[15] *https://www.malvern.com/en/products/technology/dynamic-light-scattering.*

[16] *https://www.brookhaveninstruments.com/nanobrook-90plus.*
[17] *http://pssnicomp.com/.*
[18] Harding, S.E. and Jumel, K. (1998). Light Scattering. *In*: Dunn, B.M., Ploegh, H.L., Speicher, D.W., Wingfield, P.T. and Coligan, J.E. (*eds.*), New York: John Wiley & Sons, Inc.
[19] Pecora, R. (1964). Doppler Shifts in Light Scattering from Pure Liquids and Polymer Solutions. *J. Chem. Phys.*, 40: 1604.
[20] Koppel, D.E. (1972). Analysis of macromolecular polydispersity in intensity correlation spectroscopy: The method of cumulants. *J. Chem. Phys.*, 57: 4814.
[21] Morrison, I.D., Grabowski, E.F. and Herb, C.A. (1985). Improved techniques for particle size determination by quasi-elastic light scattering. *Langmuir*, 1: 496–501.
[22] Provencher, S.W. and Stepanek, P. (1996). Global analysis of dynamic light scattering autocorrelation functions. *Part. Syst. Char.*, 13: 291–294.
[23] *https://www.agilent.com/cs/library/technicaloverviews/Public/5990-7890EN.pdf.*
[24] Rogošiæ, M., Mencer, H.J. and Gomzi, Z. (1996). Polydispersity index and molecular weight distributions of polymers. *Euro. Polym. J.*, 32: 1337–1344.
[25] Maity, P., Saha, B., Kumar, G.S. and Karmakar, S. (2016). Binding of monovalent ions with negatively charged phospholipid membranes. *Biophys. Biochim. Acta*, 1858: 706–714.
[26] Maity, P., Saha, B., Kumar, G.S. and Karmakar, S. (2016). Effect of counterions on the binding affinity of Na+ ions with phospholipid membranes. *RSC Adv.*, 6: 83916–839925.
[27] Hope, M.J.; Bally, M.B.; Webb, G.; Cullis, P.R. (1985). Production of large unilamellar vesicles by arapid extrusion procedure: Characterization of size distribution, trapped volume and ability to maintain a membrane potential. *Biophys. Biochim. Acta*, 812: 55–65.
[28] Klasczyk, B. and Knecht, V. (2011). Validating affinities for Ion–lipid association from simulation against experiments. *J. Phys. Chem. A*, 115: 10587–10595.
[29] Karmakar, S., Maity, P. and Halder, A. (2017). Charge-driven interaction of antimicrobial peptide NK 2 with phospholipid membranes. *ACS Omega*, 2: 8859–8867.
[30] Myers, D. (1999). Surfaces, Interfaces and Colloids: Principles and applications. John Wiley & Sons, Inc.
[31] Lebovka, N.I. (2014). Aggregation of charged colloidal particles. *Adv. Polym. Sci.*, 255: 57–96.
[32] Israelachvili, J.N. (2011). Intermolecular and surface forces. Elsevier and Academic Press, 3rd Ed.
[33] Corbett, J.C.W., McNeil-Watson, F., Jack, R.O. and Howarth, M. (2012). Measuring surface zeta potential using phase analysis light scattering in a simple dip cell arrangement. *Colloids Surf: Physicochemical and Engineering Aspects*, 396: 169–176.
[34] Bondos, S.E. and Bicknell, A. (2003). Detection and prevention of protein aggregation before, during, and after purification. *An. Biochem.*, 306: 223–231.
[35] Widmann, M., Trodler, P. and Pleiss, J. (2010). The isoelectric region of proteins: A systematic analysis. *PLOS One*, 5: e10546.
[36] Singh, B.P., Menchavez, R., Takai, C., Fuji, M. and Takahashi, M. (2005). Stability of dispersions of colloidal alumina particles in aqueous suspensions. *J. Colloid. Interface Sci.*, 291: 181–186.

[37] *http://pssnicomp.com/applications/isoelectric-point-iep/isoelectric-point-test/.*
[38] Vorobyov, I., Olson, T.E., Kim, J.H., Koeppe, R.E., Andersen, O.S. and Allen, T.W. (2014). On–induced defect permeation of lipid membranes. *Biophys. J.*, 106: 586–597.
[39] Lee, S.-J., Song, Y. and Baker, N.A. (2008). Molecular dynamic simulations of asymmetric NaCl and KCl solutions separated by phosphatidylcholine bilayer: Potential drops and structural changes induced by strong Na^+ lipid interactions and finite size effects. *Biophys. J.*, 94: 3565–3576.
[40] Kunz, W.; Henle, J. and Ninham, B.W. (2004). Zur Lehre von der Wirkung der Salze (About the science effect of salt) Franz Hofmeister's historical papers. *Curr. Opin. Colloid Interface Sci.*, 9: 19–37.
[41] Mclaughlin, S. (1989). Electrostatic properties of membranes. *Annu. Rev. Biophys. Biophys. Chem.*, 18: 113–136.
[42] Eisenberg, M., Gresafi, T., Riccio, T. and McLaughlin, S. (1979). Adsorption of monovalent cations to bilayer membranes containing negatively phospholipids. *Biochemistry*, 18: 5313.
[43] Elsa, Y.L., Yan, C.Y., Zhao, X. and Eisenthal, K.B. (2001). Surface potential of charged liposomes determined by second harmonic generation. *Langmuir*, 17: 2038–2066.